Available online at www.sciencedirect.com
SCIENCE DIRECT
Forest Ecology and Management 224 (2006) 81–94
Forest Ecology and Management
www.elsevier.com/locate/foreco

Use of the distributed hydrology soil vegetation model to study road effects on hydrological processes in Pang Khum Experimental Watershed, northern Thailand

Lan Cuo, Thomas W. Giambelluca *, Alan D. Ziegler, Michael A. Nullet

University of Hawaii at Manoa, Department of Geography, 2424 Maile Way, Honolulu, HI 96822, USA

Abstract

The distributed-hydrology-soil-vegetation model (DHSVM) is applied in the mountainous 94 ha Pang Khum Experimental Watershed (PKEW), northern Thailand. Climate data from August 1997 to January 2001 are used to warm up, calibrate and validate DHSVM with the existing road network explicitly represented in the model. Calibrated and tested variables are soil moisture and streamflow. The model is subsequently run again without the road, otherwise keeping parameter settings and forcing data the same. Model results with and without roads are used to study road effects on evapotranspiration, soil moisture, depth to water table, and stream discharge.

Application of DHSVM had mixed results. The model simulated soil moisture at four measurement sites and three depths very well. Streamflow was adequately estimated in only 2 of the 3 years tested, including the calibration year. The quality of the streamflow simulation may have been reduced because of year-to-year changes in land cover or water diversions not represented in the model.

Model results show that the road causes relatively small changes to averaged monthly total evapotranspiration and stream discharge in PKEW during the 3-year study period due to the low road density. Small changes in soil moisture and depth to water table occurred adjacent to and down slope of roads in PKEW. Roads increase peak flows in simulations by 3, 12, and 34%, for peak flows of less than 200, 200–800, and greater than 800 $m^3 h^{-1}$, respectively.

Keywords: Watershed modeling; DHSVM; Rural roads; Streamflow; Land use

1. Introduction

The highly compacted surfaces of unpaved roads are widely believed to alter watershed function by producing Horton overland flow (HOF), intercepting subsurface flow, and reducing travel time to the stream channel. Studies of the hydrological impacts of roads have been done at different scales, with a variety of methods, and have produced a range of results. Keppeler and Ziemer (1990) showed annual flow increases correlated with the density of roads, landings, and skid trails, which they attributed to reduced interception evaporation. Most studies, however, have found that the presence of roads does not significantly affect annual stream discharge volume (Rothacher, 1970; Harr et al., 1975; King and Tennyson, 1984; Wright et al., 1990). Many watershed studies (Harr et al., 1975; Jones and Grant, 1996; Jones, 2000) have found that roads result in higher peak flows. In some basins, observed effects on peak flows were small or undetectable (Ziemer, 1981; Wright et al., 1990; King and Tennyson, 1984). In several paired-catchment studies (Wright et al., 1990; Jones and Grant, 1996; Thomas and Megahan, 1998; Beschta et al., 2000) road effects on peak flows were important only for small events. Whereas, Jones (2000) found that road-related peak flow increases were greater for small events in two of four watershed pairs and greater for large events in the other two pairs. Detecting the effects of roads in these watershed studies was often difficult because the addition of roads was accompanied by other land cover changes, especially forest clearing.

Use of a modeling approach, on the other hand, allows the effects of roads to be isolated while controlling for precipitation intensity, soil properties, topography, and other influences on watershed response. The distributed-hydrology-soil-vegetation model (DHSVM) treats roads explicitly within a distributed, topographically-sensitive framework. Applications of DHSVM in US Pacific Northwest (PNW) watersheds have found

* Corresponding author. Tel.: +1 808 956 7390; fax: +1 808 956 3512.
E-mail address: thomas@hawaii.edu (T.W. Giambelluca).

0378-1127/$ – see front matter © 2005 Elsevier B.V. All rights reserved.
doi:10.1016/j.foreco.2005.12.009

significant road-related increases in peak flows for the largest events (Bowling et al., 2000; Storck et al., 1998; La Marche and Lettenmaier, 2001).

In montane mainland southeast Asia (MMSEA), steeply sloped lands have been cultivated for hundreds of years. The intensity and extent of cultivation has grown in recent decades in many areas, including northern Thailand, as the mountain population density increased. The rural road network in Thailand has expanded rapidly, especially in mountainous areas, despite a national ban on logging (Fox et al., 1995; Geist and Lambin, 2001). Problems with downstream water quality are routinely attributed to upland cultivation. However, mountain roads in MMSEA disrupt hydrologic and erosional processes disproportionately to their areal extent, compared with agricultural lands (Ziegler and Giambelluca, 1997; Ziegler et al., 2000; Sidle et al., 2004). Previous research in the same watershed as that used in this study has shown that roads affect streamflow mainly by generating HOF on the road surface and road margins, rather than by intercepting subsurface flow (Ziegler et al., 2001a), and road effects on stormflow are most important for frequently-occurring small events (Ziegler and Giambelluca, 1997).

The vast majority of road hydrology research has been done in the context of timber operations in the PNW, where the natural environment (climate, geology, and soils) and the types of land uses in which roads are imbedded differ with those of MMSEA. In tropical southeast Asia, snow is not a factor in runoff production, and rains are concentrated in the 6-month summer monsoon, as opposed to the Cascade Ranges of Oregon and Washington where spring snow melt often brings the highest flows and precipitation is less seasonal and tends to be highest in winter. Soils are generally deeper in MMSEA (typically >4 m) than in the PNW (usually 3 m or less) and road cuts shallower (roads are narrow and often lack an inboard ditch). Most rural roads in MMSEA are subject to daily vehicular and animal traffic throughout the year (Ziegler et al., 2001b). Mountain roads in the northwest US are used primarily for harvesting timber and often traverse steeper topography than in MMSEA.

In related work, Cuo (2005) tested DHSVM in a small watershed in northern Thailand, and used it to investigate land-cover effects on hydrological processes in that tropical montane setting. In this paper, we test DHSVM with the explicit inclusion of roads. After calibrating and testing the model, we use it to examine road effects on evapotranspiration, soil moisture, depth to water table, and stream discharge.

2. Methodology

To investigate the effects of rural roads on hydrological processes in MMSEA, we apply DHSVM within a small upland watershed in northern Thailand. Using measured meteorological time series as forcing variables, the model is calibrated and tested with respect to net radiation and soil moisture at field sites within the basin, and streamflow at the outlet. The calibrated model includes parameterization representing the existing road network in the basin. Subsequently, we remove the road from the model and run it with identical non-road parameter settings and atmospheric forcing variables to evaluate road effects on the movement and storage of water within the watershed.

2.1. Study basin

Pang Khum Experimental Watershed (PKEW; see Ziegler et al., 2004) was established in 1997 near the village of Pang Khum (19°03′N, 98°39′E), Chiang Mai Province, Thailand (Fig. 1). Our study was conducted in PKEW, a 93.7 ha basin in Mae Taeng District, which is part of the Mae Taeng River Basin. PKEW lies in the mountainous region of northern Thailand where the climate is dominated by the Indian southwest summer monsoon–northeast Asian winter monsoon system. The study area has alternating dry and wet seasons, with 90% of rainfall occurring mainly between May and November; snowfall is insignificant. Bedrock is largely granite. Soils are predominantly Ultisols of the Udic moisture regime. The original pine-dominated forest has been altered by hundreds of years of timber removal and/or swidden cultivation by Karen, Hmong, and recently, Lisu ethnic groups. Current vegetation is described by Ziegler et al. (2004). Agricultural land use is mainly swidden fields of dryland rice and vegetables planted among scattered fruit trees. The elevation of PKEW (Fig. 2) ranges from approximately 1100 to 1500 m. Slopes are between 0° and 48° based on a 5 m DEM.

Roads in PKEW are not paved, have no subgrade, were built over existing footpaths or animal trails, and generally do not have road-side ditches. Motorcycles, trucks, cattle and pedestrians are common users of the roads in PKEW. The

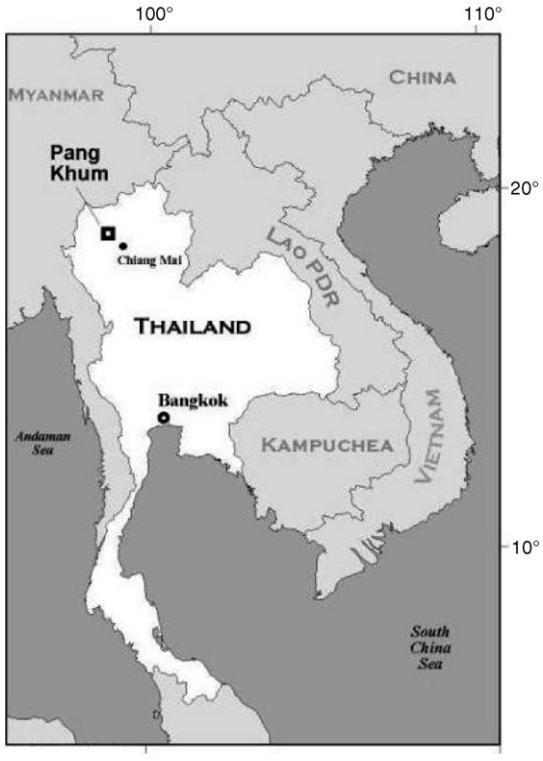

Fig. 1. Location of Pang Khum Experimental Watershed.

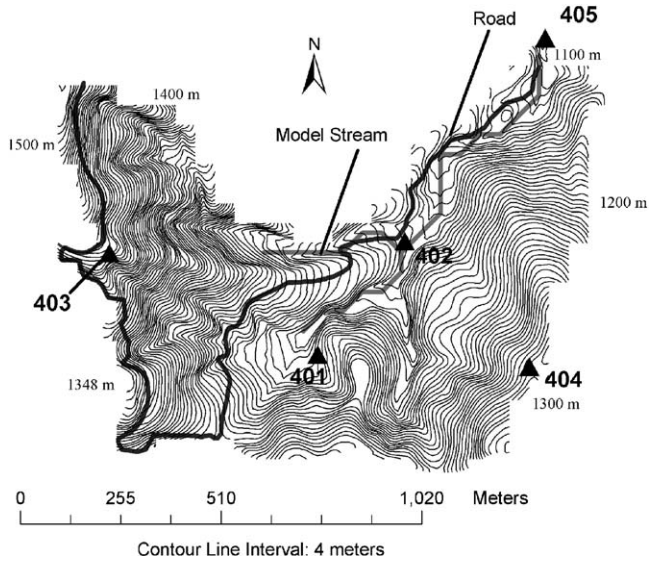

Fig. 2. Four-meter-interval contour map of PKEW. 401 and 402 are climate stations, 403 and 404 are rainfall and soil moisture stations, 405 is the stream gauge, bold line represents road, gray line represents model stream.

portion of the road along the western and southern boundaries of the watershed (Fig. 2) traverses a steep hillslope and has a variable cutbank height ranging from 0 to more than 4 m. Some sections have deeply eroded gullies on the road surface, which developed from wheel ruts; other sections of the road have sparse vegetation on the road crown between bare, compacted wheel tracks. Overland flow on the western portion either routes to lower road sections or to the hillslope. There are no culverts on this part of the road. Gullies are evident on hillslopes where overland flow exits the road. The portion of the road from the southern boundary to the northeastern corner is routed down the axis of the valley, crossing the stream several times (culverts are found at stream crossings). Most of this part of the road has a sparsely vegetated road crown with bare, compacted wheel tracks. The cutbank here is generally less than 1 m high. Surface flow on this portion of the road routes to the stream channel (at culverts) or to the hillslope. Generally, roads on steep slopes (e.g. along the western boundary) are wider than elsewhere. Usually, material removed during road construction is pushed downslope where it becomes revegetated over time, hence fillslopes are not included as part of the road area here. The total road area including road surface and road cutbank area is estimated to be 12,294 m^2, or about 1.2% of the PKEW drainage area. About 96% of total road area is located on slopes exceeding 10% (5.7°).

2.2. Field measurements

PKEW has two fully-equipped climate stations (401 and 402) over advanced secondary forest and swidden agriculture sites, respectively, two stations measuring only soil moisture (403 and 404), and a stream gauge station (405) (Fig. 2). Table 1 summarizes time-dependent measurements at PKEW field stations. All sensors at stations 401, 402, 403, and 404, except raingages, were sampled on a 10 s interval and means were recorded on a 20 min interval. Rainfall was recorded on a 1 min interval, and the height of water behind a broad-crested v-notch weir at station 405 was recorded whenever a significant change occurred. The theoretical rating curve for the weir, used to estimate stream discharge ($m^3\ s^{-1}$) on the basis of stage (height of water), was verified with numerous manual measurements of flow at a range of flow magnitudes. All data were subsequently aggregated to hourly intervals for use in the model. Model forcing and calibration variables are listed in Table 1.

2.3. Model

DHSVM accounts for the effects of topography and land cover, including roads, by explicitly representing the spatial distribution of stream and road networks, stream and road morphology, soil properties, soil depth, vegetation properties, and elevation. Digital elevation data are used in the model for flow routing, estimation of soil depth distribution, and meteorological data extrapolation. Each cell can have up to two vegetation layers, and a user-specified number of soil layers. DHSVM incorporates canopy precipitation interception, evapotranspiration, energy and radiation balance, snow accumulation and melt, runoff generation through saturation excess and infiltration excess mechanisms, unsaturated soil moisture movement, saturated subsurface flow, and ground

Table 1
Time-dependent field measurements at field sites in PKEW

Variable	Sensor	Location(s)	Purpose
Net radiation	REBS Q*7[a]	401, 402	Calibration
Downward shortwave radiation	Eppley 8-48[b]	401, 402	Forcing
Reflected shortwave radiation	Eppley 8-48[b]	401, 402	Forcing[c]
Surface temperature	Everest 4000[d]	401, 402	Forcing[c,e]
Air temperature	Vaisala HMP45C[f]	401, 402	Forcing
Relative humidity	Vaisala HMP45C[f]	401, 402	Forcing
Wind speed	MetOne 034A[g]	401, 402	Forcing
Soil temperature	Campbell Sci. TVAR[h]	401, 402	Forcing
Soil moisture (at 3 depths)	Campbell Sci. CS615[h]	401, 402, 403, 404	Calibration
Rainfall	Texas Electronics TE525[i]	401, 402, 403, 404	Forcing
Stream discharge	Druck PDCR-1830-8335[j]	405	Calibration

[a] Radiation and Energy Balance Systems, Seattle, WA, USA.
[b] Eppley Laboratory, Newport, RI, USA.
[c] Reflected shortwave radiation and surface temperature are used together with net radiation and downward shortwave radiation to estimate downward longwave radiation, a forcing variable.
[d] Everest Interscience, Tucson, AZ, USA.
[e] Surface temperature is converted to upward longwave radiation using the Stefan–Boltzmann equation.
[f] Vaisala, Helsinki, Finland.
[g] MetOne, Grants Pass, OR, USA.
[h] Campbell Scientific, Logan, UT, USA.
[i] Texas Electronics, Dallas, TX, USA.
[j] Druck, New Fairfield, CT, USA; sensor measures height of water behind broad-crested v-notch weir.

Table 2
Land cover and soil classes in PKEW

Land-cover classes	Soil classes
1. Rice paddy	1. Valley rice field soil
2. Swidden field (402)[a]	2. Valley swidden field soil (402)
3. Tilled field	3. Valley tilled field soil
4. Fallow field	4. Valley fallow field soil
5. Young secondary forest (403)	5. Valley young secondary forest soil
6. Advanced secondary forest (401, 404)	6. Valley advanced secondary forest soil (401)
	7. Ridge fallow field soil
	8. Ridge young secondary forest soil (403)
	9. Ridge advanced secondary forest soil (404)

[a] Numbers in parentheses are station codes to show land cover and soil classes at each station.

water recharge and discharge. A detailed description of DHSVM can be found in Wigmosta et al. (1994, 2002), Storck et al. (1998), and Nijssen and Lettenmaier (1999).

Model parameters fall under soil, vegetation (land cover), elevation, stream channel and road networks, and radiation categories. The spatial framework of the model is set by a digital elevation model (DEM) of user-defined resolution (50 m in our case). Any number of soil and land-cover classes can be defined. Soil and land-cover classes are then assigned to each cell. Stream channel and road segment information is vector-based, with links to the underlying grid. The spatial distribution of downward shortwave radiation incident on inclined hillslopes is computed from digital elevation data.

2.4. PKEW initial parameter settings

Land-cover classes are listed in Table 2. Parameter values for each land-cover class were initially set based on field measurements, literature values, and model defaults; some parameters were subsequently changed during calibration (Table 3).

Land-cover units in PKEW were mapped during December 2000 and January 2001. Field boundaries were surveyed by walking each boundary while a Trimble GeoExplorer III GPS unit (Trimble Navigation Limited, Sunnyvale, CA) recorded data every 1 s. Data collected from the GPS unit were then downloaded into Pathfinder Office software (Trimble Navigation Limited, Sunnyvale, CA) and differentially corrected with data from a base station established nearby (~2 km from PKEW). Data were then converted into shapefile format, ported to ArcView 3.1 (ESRI), and adjusted to generalize the field boundaries, removing GPS errors created from large trees and steep local topography.

Measurements throughout the basin (Giambelluca, 1996; Ziegler and Giambelluca, 1997) reveal the strong influence of land use on soil hydraulic properties. Based on our observations, we characterized the spatial variability in soil properties as a function of land-cover class and topographic position within the basin—ridge versus valley (Table 2). Initial parameter settings for each soil class were based on field measurements, literature values, and model defaults; some parameter values were modified during calibration (Table 4).

To facilitate calibration, three soil layers were used with a vertical distribution corresponding to the depths of soil moisture sensors: 0–0.3, 0.3–0.9, and 0.9–1.5 m below surface.

Table 3
DHSVM vegetation parameter values after calibration

Vegetation parameters[a]	Vegetation class[b]							
	1	2	3	4	5		6	
					Understory	Overstory	Understory	Overstory
Impervious ground fraction [a]	0.0	0.0	0.0	0.0		0.0		0.0
Canopy overstory fractional coverage [b]						0.6		0.9
Trunk space (fraction) [b]						0.4		0.5
Canopy hemisphere fractional coverage [b]						0.6		0.9
Aerodynamic extinction factor for wind through the overstory (fraction) [a,d]						0.5		1.5
Clumping factor [a]						0.4		0.5
Leaf angle A/B [a]						0.5/0		0.5/0
Scattering parameter (fraction) [a]						0.8		0.6
Overstory/understory vegetation height (m) [b]	0.5	2.0	2.0	2.0	2.0	10.0	2.0	15.0
Maximum/minimum stomatal resistance (s/m) [a,d]	3100/50	2000/240	2500/230	2500/230	2100/180	2100/180	2500/220	2500/220
Light level where stomatal resistance equals two times the minimum stomatal resistance (R_{pc}, fraction) [a]	0.108	0.108	0.108	0.108	0.108	0.108	0.108	0.108
Soil moisture threshold below which transpiration is restricted (fraction) [c,d]	0.45	0.20	0.20	0.10	0.18	0.18	0.25	0.25
Vapor pressure deficit above which transpiration is restricted (Pa) [a,d]	5000	3500	6000	6000	4050	4050	4050	4050

[a] Given in square brackets are the sources of the initial parameter settings—a: model default; b: field observation; c: Giambelluca (1996) and Ziegler (2000); d: initial settings subsequently modified during calibration.
[b] Class 1: rice paddy; class 2: swidden field; class 3: tilled field; class 4: fallow field; class 5: young secondary forest; class 6: advanced secondary forest.

The distribution of total soil depth in PKEW initially was generated based on the DEM using an ArcInfo (ESRI, Inc.) macro language (AML) script provided by the DHSVM modeling group (University of Washington). Soil depth was subsequently adjusted during calibration.

The stream network for the watershed is defined from the DEM using ArcInfo. The DHSVM modeling group (University of Washington) provided an AML script to generate the model stream morphology and network files from the DEM-defined stream network. Adjustments were made in order to bring the modeled network into agreement with field survey-based information. Flow routing on road surface was also guided by field observation. Roads were divided into 50 segments in order to reflect changing characteristics. Stream and road class parameters are based on field observation.

2.5. Calibration and testing procedures

Model calibration and testing were done by optimizing model simulation of net radiation at sites 401 and 402, soil moisture in three soil layers at sites 401, 402, 403, and 404, and streamflow (405). Parameter adjustments were made to reduce differences between simulated and observed values, starting with net radiation. The calibration period is from 1 February 1998 to 31 December 1998. The validation period is from 1 January 1999 to 3 January 2001. Two gaps in the forcing data, 28 June–3 August 1999 and 7 January–27 February 2000, were filled with mean values of the periods 1 month before and after each gap. Model output for these gaps was excluded from subsequent analysis. Measurements from 1 August 1997 to 31 January 1998 were used to warm up the model for the

Table 4
DHSVM soil parameter values after calibration

Soil parameters[a]	Soil class[b]								
	1	2	3	4	5	6	7	8	9
Lateral saturated hydraulic conductivity (×E − 5 m/s) [c,g]	0.00015	2.5	2.8	0.30	2.7	3.5	0.35	2.8	3.5
Exponential decrease rate of lateral saturated hydraulic conductivity [d,g]	0.1	0.1	0.3	0.1	0.5	0.1	0.7	0.5	0.5
Maximum infiltration rate (×E − 5 m/s) [c,g]	0.0002	1.5	1.8	0.25	2.0	3.0	0.2	2.5	3.0
Soil surface albedo [a]	0.25	0.15	0.25	0.25	0.15	0.25	0.25	0.15	0.20
Porosity (fraction, three soil layers) [e,g]	0.5488	0.575	0.5795	0.5969	0.5507	0.5215	0.5469	0.5005	0.5405
	0.5285	0.489	0.5495	0.5879	0.5475	0.3905	0.4969	0.3795	0.4295
	0.5185	0.437	0.5395	0.5800	0.5375	0.3555	0.4900	0.3495	0.3875
Field capacity (fraction, three soil layers) [b,g]	0.255	0.330	0.305	0.235	0.210	0.305	0.305	0.210	0.364
	0.285	0.406	0.345	0.235	0.275	0.305	0.285	0.275	0.374
	0.305	0.411	0.365	0.235	0.264	0.305	0.285	0.284	0.345
Wilting point (fraction, three soil layers) [b,g]	0.1354	0.149	0.108	0.200	0.128	0.165	0.1400	0.179	0.255
	0.1375	0.281	0.135	0.203	0.238	0.225	0.1830	0.180	0.265
	0.1390	0.325	0.145	0.204	0.243	0.219	0.1940	0.176	0.246
Pore size distribution index (three soil layers) [f]	0.1404	0.1404	0.1404	0.1404	0.1404	0.1404	0.1404	0.1404	0.1404
	0.1404	0.1650	0.1404	0.1404	0.1404	0.1404	0.1404	0.1404	0.1404
	0.1174	0.1740	0.1174	0.1174	0.1404	0.1174	0.1404	0.1404	0.1404
Bubbling pressure (m, three soil layers) [f]	0.2808	0.2808	0.2808	0.2808	0.2808	0.2808	0.2808	0.2808	0.2808
	0.2808	0.3808	0.2080	0.2808	0.2808	0.2808	0.2808	0.2808	0.2808
	0.2589	0.3889	0.2589	0.2589	0.2808	0.2589	0.2808	0.2808	0.2808
Vertical saturated hydraulic conductivity (×E − 5 m/s, three soil layers) [b,g]	0.0001	2.5	2.8	0.3	4.5	3.0	0.3	4.5	4.5
	0.0002	0.18	0.06	0.025	0.05	0.75	0.025	0.050	0.080
	0.0002	0.128	0.058	0.024	0.048	0.60	0.024	0.048	0.066
Bulk density (kg/m^3, three soil layers) [b]	1160	1470	1240	1090	1270	1040	1090	1270	1040
	1280	1489	1360	1210	1390	1160	1210	1390	1160
	1450	1560	1530	1380	1660	1330	1380	1660	1330
Soil thermal capacity (×E6 J/(m^3 K), three soil layers) [a]	1.4	1.4	1.4	1.4	1.4	1.4	1.4	1.4	1.4
	1.4	1.4	1.4	1.4	1.4	1.4	1.4	1.4	1.4
	1.4	1.4	1.4	1.4	1.4	1.4	1.4	1.4	1.4
Soil thermal conductivity (W/(m K), three soil layers) [a]	7.114	7.114	7.114	7.114	7.114	7.114	7.114	7.114	7.114
	6.923	6.923	6.923	6.923	6.923	6.923	6.923	6.923	6.923
	6.923	6.923	6.923	6.923	6.923	6.923	6.923	6.923	6.923

[a] Given in square brackets are the sources of the initial parameter settings: a: model default; b: Giambelluca (1996) and Ziegler (2000); c: assumed to be the same as the first layer vertical saturated hydraulic conductivity, Giambelluca (1996) and Ziegler (2000); d: calculation from measured saturated hydraulic conductivity in shallow layers; e: calculated from bulk density; f: Riparian Ecosystem Management Model (REMM) User Guide, and Clapp and Hornberger (1978); g: initial settings subsequently modified during calibration.

[b] Class 1: valley rice paddy soil; class 2: valley swidden field soil; class 3: valley tilled field soil; class 4: valley fallow field soil; class 5: valley young secondary forest soil; class 6: valley advanced secondary forest soil; class 7: ridge fallow field soil; class 8: ridge young secondary forest soil; class 9: ridge advanced secondary forest soil.

calibration period runs. The warm-up run was initiated with soil moisture set at 0.3 $m^3\ m^{-3}$ and other state variables set at zero. Model state variables at the end the calibration period were carried over to initialize runs for the validation period.

Some parameters influencing one variable (e.g. soil moisture) also influence one or both of the others (net radiation and streamflow), and, as a result, optimization of each was not entirely independent of the others. Calibration was, therefore, iterative, and proceeded as follows. Vegetation parameters such as albedo were adjusted at stations 401 and 402 to obtain a reasonable estimation of net radiation. Sensitive soil parameters were then calibrated to optimize soil moisture simulations at the four stations. Finally, streamflow was tuned. At each stage in the calibration, checks were done and parameters were readjusted to minimize negative effects of recent parameter shifts on previously optimized variables.

Not all land cover and soil classes are represented by our recording field stations. Therefore direct calibration of the properties of those classes was not possible. Parameters for these land covers were adjusted during the streamflow calibration, but we limited the adjustment of each parameter, keeping it within its known (based on field observations) or assumed (based on literature) range. In general, parameter values of classes without calibration data were adjusted in such a way that known or assumed relative differences among classes were preserved.

To reduce subjectivity in the evaluation of model performance, goodness-of-fit statistics were used to identify the optimal parameter settings during calibration. The quality of the resulting simulations was assessed by comparing root mean square errors (RMSEs) of daily soil moisture and streamflow estimates with their respective measurement variabilities, where:

$$\mathrm{RMSE} = \sqrt{\frac{1}{N}\sum_{i=1}^{N}(s_i - o_i)^2} \tag{1}$$

where N is the sample size, s_i the simulated value, and o_i is the observed value.

This method was used by Wigneron et al. (1999) to evaluate the interactions between Soil–Biosphere–Atmosphere (ISBA) model. Standard deviation (S.D.), and median absolute deviation (MAD) were used to quantify measurement and simulation variability. Bias, the percent error in total stream discharge, and model efficiency (Nash and Sutcliffe, 1970) were used as basic measures of streamflow simulation skill. Model efficiency (ME) is defined as:

$$\mathrm{ME} = 1 - \varepsilon_s \tag{2}$$

where

$$\varepsilon_s = \frac{\sigma_\varepsilon^2}{\sigma_o^2}$$

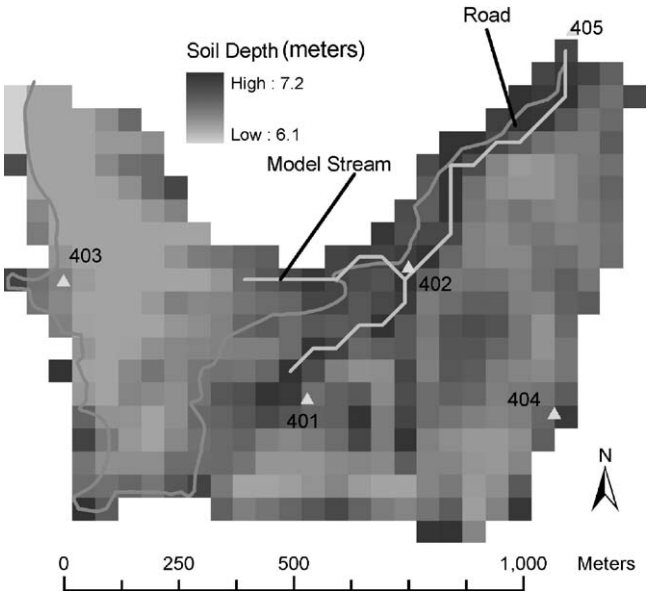

Fig. 3. Model soil depth distribution in PKEW.

where

$$\sigma_\varepsilon^2 = \frac{1}{N-1}\sum_{i=1}^{N}(s_i - o_i)^2$$

and where σ_o^2 = variance of observed data.

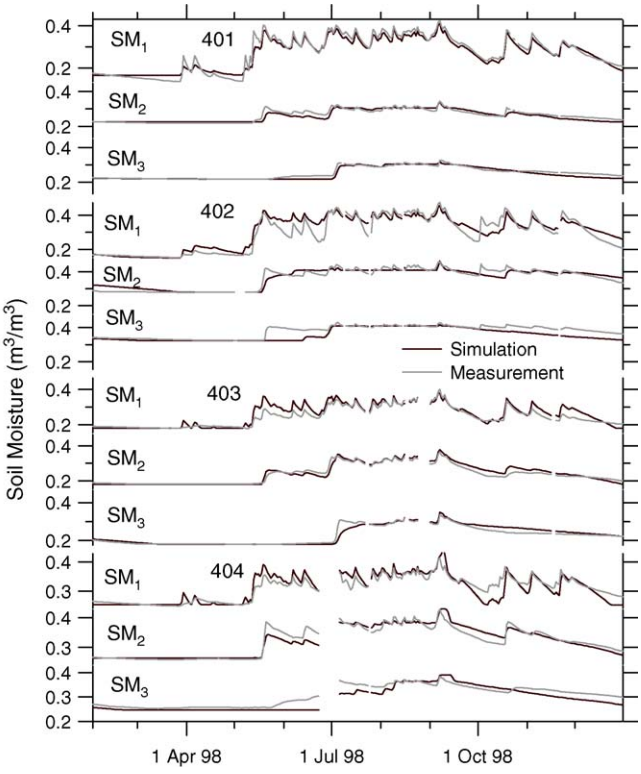

Fig. 4. Daily soil moisture simulation and measurement at stations 401, 402, 403, and 404 during calibration period; SM_1: first layer (0–0.3 m); SM_2: second layer (0.3–0.9 m); SM_3: third layer (0.9–1.5 m).

Calibrated DHSVM vegetation and soil parameter values are listed in Tables 3 and 4. Monthly albedo and leaf area index values, not shown in Table 3, were initially set based on Larkin (2002) and Giambelluca (1996), respectively, and subsequently, adjusted during calibration. Model soil depths (Fig. 3), derived through calibration, are 1–3 m deeper than those observed in the basin.

3. Simulation results

Optimization of net radiation will be presented in a separate paper (Cuo, 2005). Below we describe model calibration and testing with respect to soil moisture and streamflow.

3.1. Calibration period

The 11-month calibration period includes the entire rainy season of 1998. Time series graphs indicate that soil moisture is generally simulated well during the calibration period at the four field station sites, for all three soil layers (Fig. 4). RMSE values and comparison of the statistics of measured and simulated soil moisture (Table 5) confirm that the model was able to represent soil moisture variation with reasonable accuracy. Station 402, the swidden agriculture site, had the poorest simulation (RMSE = 0.02–0.04 $m^3\ m^{-3}$) perhaps due to the frequent changes in vegetative cover at the site associated with the farmer's crop rotation schedule, alternating fallow periods, and burning episodes. In the model, we did not attempt to replicate the effects of these land-use activities.

During model calibration, simulated total stream discharge was kept as close as possible to the measured total, while also minimizing RMSE between simulated and measured streamflow. Baseflow is consistently underestimated throughout the simulation period prior to the large event peaking on 5 September, and consistently overestimated after that (Fig. 5). Storm peaks are underestimated before 5 September. Table 6 shows that while total discharge is correctly estimated (bias = 0), RMSE is 540 $m^3\ d^{-1}$ or 70% of the measured mean. Model efficiency, 0.51, is acceptable, but generally lower than in previous applications of DHSVM.

Various attempts were made to improve the streamflow simulation. For example, the estimate could be improved significantly if the use of unrealistic vegetation and soil parameter values were permitted for certain land covers; however, this was not done in order to maintain parameter settings that were reasonable representations of the various land

Table 5
Statistics of soil moisture simulation and measurement at four stations during calibration and validation periods

Station	Soil layer	RMSE[a] ($m^3\ m^{-3}$)	Mean (S.D.[b]) ($m^3\ m^{-3}$)		Median (MAD[c]) ($m^3\ m^{-3}$)	
			Measurement	Simulation	Measurement	Simulation
Calibration period						
401	1	0.02	0.27 (0.08)	0.27 (0.07)	0.29 (0.07)	0.28 (0.06)
	2	0.01	0.26 (0.03)	0.26 (0.03)	0.26 (0.03)	0.25 (0.02)
	3	0.01	0.25 (0.03)	0.25 (0.03)	0.24 (0.03)	0.23 (0.00)
402	1	0.04	0.29 (0.10)	0.30 (0.09)	0.31 (0.10)	0.34 (0.05)
	2	0.02	0.36 (0.06)	0.36 (0.05)	0.38 (0.03)	0.39 (0.02)
	3	0.03	0.38 (0.04)	0.36 (0.04)	0.39 (0.02)	0.35 (0.02)
403	1	0.02	0.24 (0.05)	0.26 (0.06)	0.24 (0.05)	0.26 (0.06)
	2	0.01	0.24 (0.05)	0.24 (0.06)	0.23 (0.04)	0.24 (0.06)
	3	0.01	0.22 (0.05)	0.23 (0.05)	0.22 (0.04)	0.22 (0.05)
404	1	0.02	0.31 (0.04)	0.31 (0.05)	0.32 (0.03)	0.31 (0.05)
	2	0.01	0.32 (0.05)	0.32 (0.05)	0.32 (0.05)	0.32 (0.05)
	3	0.02	0.30 (0.04)	0.29 (0.05)	0.31 (0.04)	0.28 (0.04)
Validation period						
401	1	0.04	0.32 (0.08)	0.29 (0.07)	0.35 (0.04)	0.31 (0.05)
	2	0.01	0.28 (0.04)	0.27 (0.04)	0.29 (0.03)	0.30 (0.01)
	3	0.01	0.28 (0.04)	0.27 (0.04)	0.30 (0.02)	0.30 (0.01)
402	1	0.05	0.32 (0.10)	0.34 (0.07)	0.36 (0.07)	0.37 (0.05)
	2	0.02	0.38 (0.06)	0.37 (0.05)	0.41 (0.03)	0.40 (0.01)
	3	0.01	0.39 (0.03)	0.38 (0.04)	0.41 (0.02)	0.41 (0.01)
403	1	0.04	0.29 (0.08)	0.28 (0.06)	0.31 (0.06)	0.31 (0.03)
	2	0.02	0.28 (0.07)	0.27 (0.07)	0.32 (0.04)	0.31 (0.03)
	3	0.02	0.26 (0.06)	0.26 (0.06)	0.29 (0.03)	0.29 (0.02)
404	1	0.04	0.35 (0.06)	0.33 (0.05)	0.36 (0.05)	0.35 (0.03)
	2	0.01	0.34 (0.06)	0.34 (0.06)	0.37 (0.03)	0.38 (0.02)
	3	0.01	0.33 (0.05)	0.32 (0.05)	0.35 (0.02)	0.35 (0.02)

[a] RMSE: root mean square error.
[b] S.D.: standard deviation.
[c] MAD: median absolute deviation.

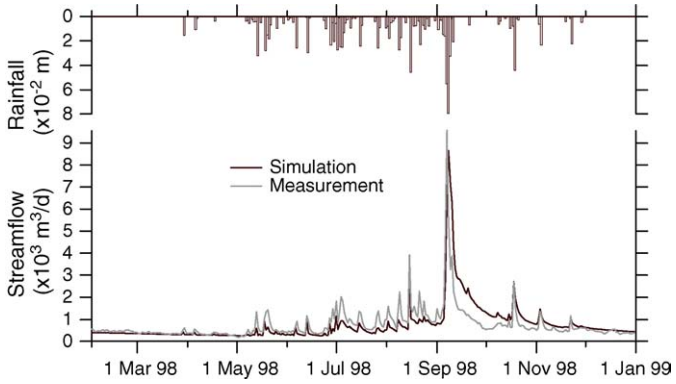

Fig. 5. Simulated and measured daily streamflow during calibration period.

covers. It was also found that the streamflow simulation could be improved at the expense of the soil moisture simulations. Instead, it was deemed more important to maintain parameter settings that best described the distributed, land-use-specific characteristics of the basin.

In calibrating the streamflow estimate, it became clear that the accuracy of either baseflow or peak flow estimates could be improved, but not both. Recently, Beckers and Alila (2004) suggested that tradeoffs between accurate simulation of peak flows and baseflow in DSHVM occur because preferential flow is not explicitly represented in the model.

3.2. Assessment

The 2-year validation period includes the rainy seasons of 1999 and 2000. Time series graphs (Fig. 6) indicate that soil moisture simulation at the four sites is very reasonable, as it was during the calibration period. In Table 5, daily-interval RMSE values are generally similar or slightly higher than the corresponding calibration period values.

Average rainfall and streamflow during the 2 years of the validation period were much higher than during the calibration period (Table 6 and Fig. 7). The streamflow simulation during the validation period was generally poor, especially for 1999. On average the simulation overestimated measured streamflow by 58% during 1999 and underestimated flow by 9% during 2000. Model efficiency was very low in 1999.

3.3. Model evaluation and sources of error

Model efficiencies for the streamflow estimate during the validation period are low compared with those of prior applications of the model (e.g. 0.57–0.87, Beckers and Alila, 2004; 0.84–0.91, Thyer et al., 2004; 0.41–0.86, Leung et al., 1996; 0.89, Wigmosta and Burges, 1997). Error in the streamflow simulation could have resulted from one or more of the following: (1) the large difference in precipitation between the calibration and validation periods; (2) two data gaps during the 1999 wet season; (3) the relatively coarse 50 m DEM, which determines the spatial resolution of land cover and soil representation, and influences the topographically-driven surface and subsurface water flow; (4) year-to-year changes in land cover or water diversion during the study period (the land cover pattern, based on a December 2000–January 2001 survey, was held constant in the model throughout the simulation periods); (5) errors in meteorological forcing data or stream discharge measurements; (6) inadequate representation of subsurface and surface flow processes in the model.

Failure of the 50 m DEM to capture topographic complexity may contribute to errors in the simulation, but this does not explain the interannual differences in model performance. The divergence between simulated and measured streamflow is much greater during 1999 than either 1998 or 2000. This may be partly explained by the out-of-calibration-range (wetter) conditions, and the effects of the two data gaps on the simulation. Precipitation for 2000 (1595 mm; 299 days of record) and 1999 (1691 mm; 308 days of record) is high compared with 1998 (1140 mm; 334 days of record). In fact, 1999 was an exceptionally wet year considering that the 1691 mm total is missing all of the wet season month of July. As a general rule, the runoff coefficient, the ratio of stream discharge (Q) to precipitation (P), increases for a given watershed with increasing P. But, while the measured runoff coefficient was 0.43 for 2000, it was only 0.26 for 1999, identical to the runoff coefficient in the much drier year of 1998. This suggests one of three possible problems: (1) substantial error exists in the 1999 streamflow measurement; (2) low antecedent moisture conditions following the dry year of 1998 caused a reduction in the 1999 runoff coefficient; or (3) unrepresented land cover or water diversion changes caused a

Table 6
Statistics of observed and simulated stream discharge during calibration and validation periods

	RMSE[a] ($m^3\ d^{-1}$)	Mean (S.D.[b]) ($m^3\ d^{-1}$)		Median (MAD[c]) ($m^3\ d^{-1}$)		Bias[d] (%)	Model efficiency[e]
		Measurement	Simulation	Measurement	Simulation		
Calibration	540	766 (774)	763 (907)	536 (159)	506 (198)	0	0.51
Validation							
1999	1542	1321 (1095)	2093 (2289)	1187 (877)	1095 (790)	58	−0.76
2000	969	2125 (1096)	1937 (1517)	1935 (563)	1534 (839)	−9	0.31

[a] RMSE: root mean square error.
[b] S.D.: standard deviation.
[c] MAD: median absolute deviation.
[d] Bias: error in total.
[e] Model efficiency according the Nash and Sutcliffe (1970).

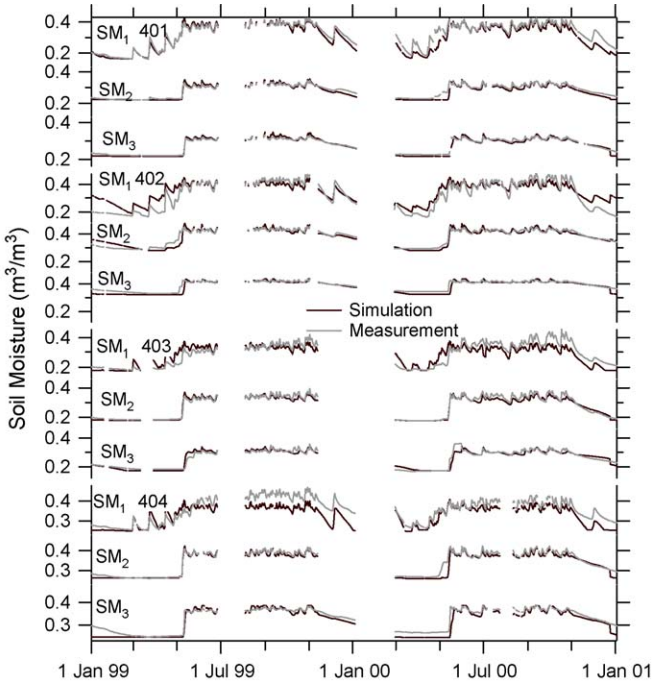

Fig. 6. Daily soil moisture simulation and measurement at stations 401, 402, 403, and 404 during validation period; SM_1: the first layer (0–0.3 m); SM_2: the second layer (0.3–0.9 m); SM_3: the third layer (0.9–1.5 m).

reduction in streamflow in 1999. Manual stage measurements taken numerous times throughout the 1999 wet season give strong support for the accuracy of the automated stage measurement. No significant changes in the weir or the stream channel above the weir were observed that may have altered the stage–discharge relationship. Regarding the second possibility, many studies have shown the effects of antecedent moisture conditions on runoff coefficients (e.g. Noguchi et al., 2001). However, the low water status of the basin before the start of the 1999 rainy season is correctly simulated by the model, as indicated by the close correspondence of simulated and observed soil moisture and streamflow. Hence, we suspect the poor streamflow simulation during the rainy season stems from land cover changes and/or water diversions not represented in the model for 1999. While year-to-year changes during the study period (e.g., opening and closing of rice paddies), which may have had significant short-term impacts on streamflow, were not monitored carefully, some changes are known to have occurred. For example, a substantial area in the lower part of PKEW was converted to rice paddy, then subsequently returned to dryland agriculture during the study (timing and land area involved were not recorded).

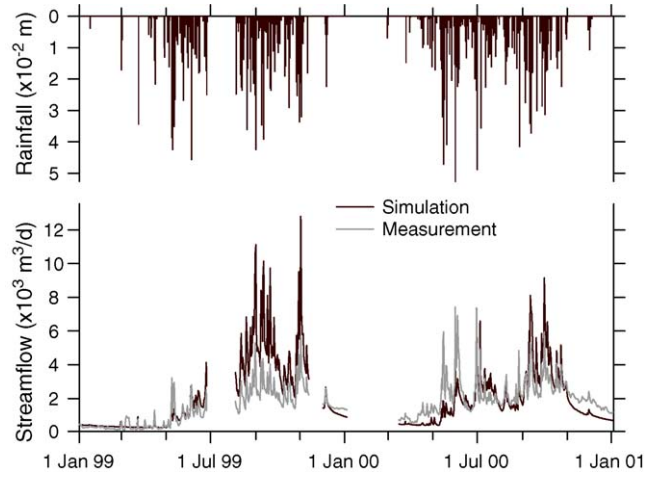

Fig. 7. Daily streamflow simulation and measurement during validation period.

Soil moisture results are reasonably good throughout the 3-year study period at all four sites, at all depths. The streamflow simulation is acceptable in two of the model years, and poor in the other year. If our suspicions regarding the effects of temporary land cover changes are correct, then the fundamental soundness of the model is not threatened by the poor simulation in 1999. On this basis, we cautiously accept the model validation and use the model to investigate the effects of roads on watershed processes.

3.4. Road effects

3.4.1. Water balance

Road effects are examined first by comparing monthly results for road and non-road simulations. Fig. 8 gives mean monthly values of each component of the water balance for the entire study period, including calibration and validation periods. Monthly ET is slightly lower for the road simulation during all months except January. The changes range from −1.12% in February to +0.71% in January. Stream discharge is consistently higher with roads for wet season months (May–November), with an average change of +3.3%, and slightly lower for dry season months, averaging −1.4%. Higher wet season streamflow with roads is explained by approximately equal reductions of ET and storage change (either less storage increase or greater storage loss during a month).

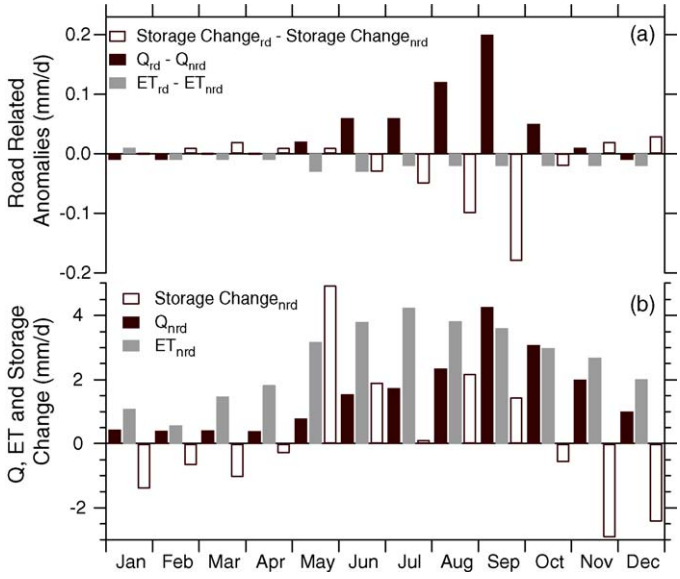

Fig. 8. Road-related anomalies (road minus non-road) in streamflow, ET and storage change during February 1998 through December 2000: (a) mean monthly anomalies; (b) mean monthly non-road fluxes.

3.4.2. Soil moisture

Fig. 9 shows the spatial distribution of the road-related anomaly (road minus non-road value in each cell) in first-layer soil moisture averaged for two 8-day periods, one wet (1–8 September 1998, rainfall = 217 mm) and one dry (1–8 December 1998, rainfall = 0 mm). For the wet period (Fig. 9a), the road resulted in a redistribution of upper-layer soil moisture near and down slope of the road, with the largest changes occurring down slope of the road in the southwest corner. In general, cells with reduced soil moisture occur on or near roads, while cells with increased soil moisture are found down slope of ''sinks'', locations where on-road flow converges. The road–non-road difference for this period averages close to zero, with soil moisture higher in 109 of the total 375 cells and lower in 62 cells (remaining cells had no change). The range of soil moisture anomaly (-0.02 to $0.13\ m^3\ m^{-3}$) represents shifts of -6 to $+37\%$ in relation to typical wet season soil moisture values of approximately $0.35\ m^3\ m^{-3}$. The pattern of soil moisture disturbance due to roads persists into the dry season (Fig. 9b). Again, the soil moisture anomaly averaged near zero, with 74 cells having higher values and 88 cells lower values with roads.

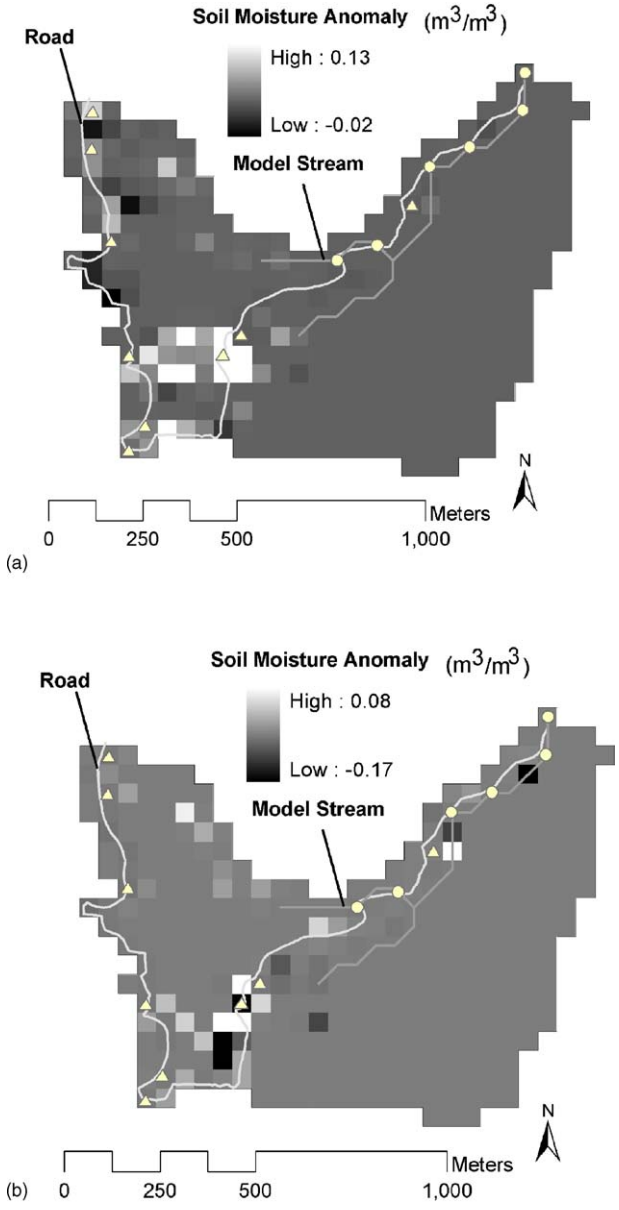

Fig. 9. Spatial distribution of road-related anomalies (road minus non-road) in soil moisture for two sample periods: (a) wet: 1–8 September 1998 and (b) dry: 1–8 December 1998. Triangles represent road sinks (points where on-road flow converges). Circles show the locations of culverts. Broad areas of uniform medium gray are cells with no change.

Fig. 10 shows the daily time series of basin-averaged, road-related soil moisture anomaly in each soil layer, for the calibration and validation periods. In general, basin-averaged soil moisture is affected only slightly by the road, in each layer. In layer 1, soil moisture is increased by roads during the middle of the wet season. In layers 2 and 3, the road results in lower soil moisture in the late part of the wet season.

3.4.3. Depth to water table

Depth to water table anomalies for the previously identified 8-day wet and dry sample periods are shown in Fig. 11. During the wet period, the water table is generally farther below the surface near the road in the lower part of the basin, and closer to the surface in areas down slope of sinks on the upper part of the road. Averaging over the whole basin, the water table is approximately 3 cm closer to the surface with the road, with the water table deeper beneath the surface for 115 cells and closer to the surface for 130 cells. The anomaly pattern for the dry period is similar to that of the wet period. On average for the whole basin during the dry period, the water table is essentially unchanged (1 mm deeper beneath the surface) with roads, with the depth to water table greater for 128 cells and less for 116 cells. Effects of roads on daily aggregated basin-averaged depth to water table over the 3-year study period are shown in Fig. 12. In general, the water table is lower with roads, except during the middle of each wet season.

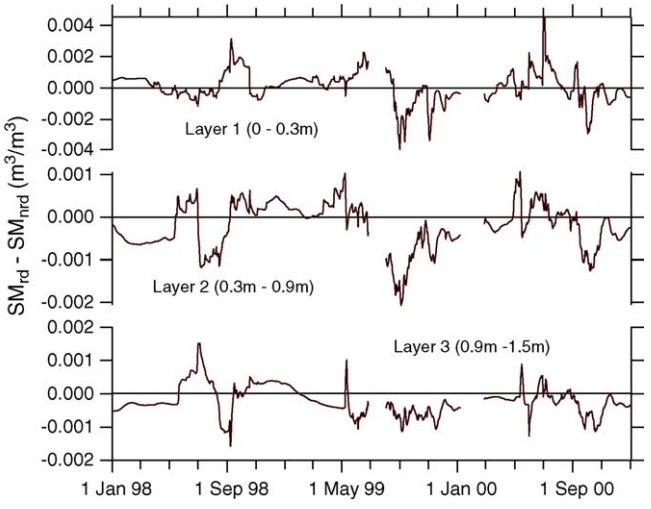

Fig. 10. Time series of basin-averaged road-related soil moisture anomaly (road minus non-road) in each soil layer.

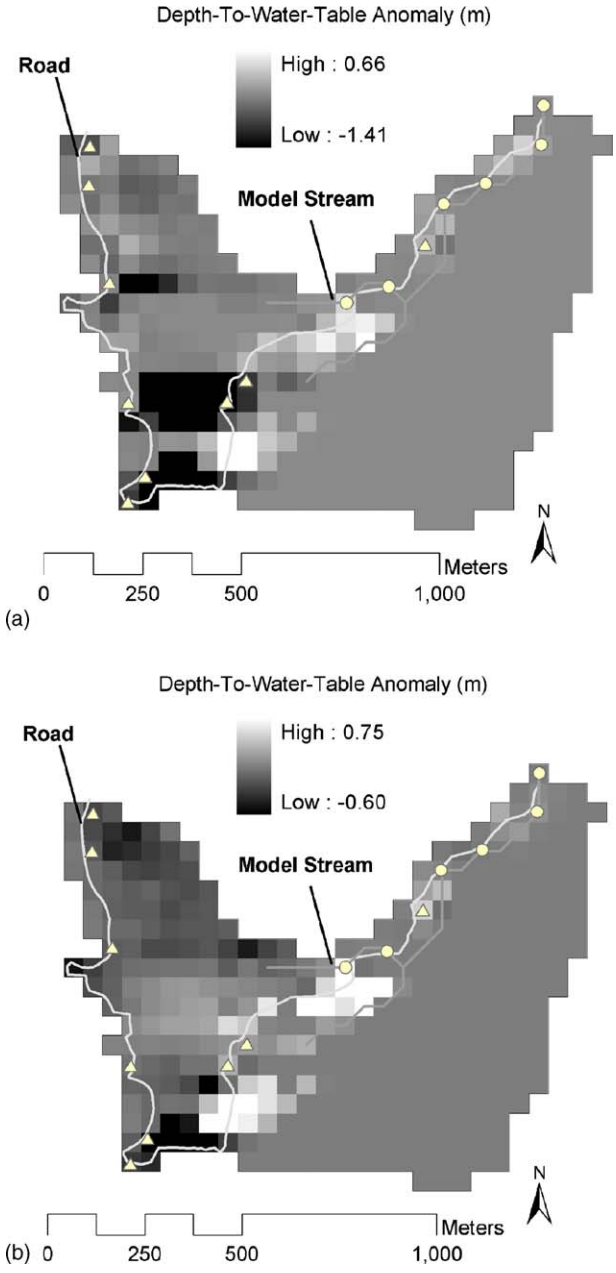

Fig. 11. Spatial distribution of road-related anomalies (road minus non-road) in depth to water table for two sample periods: (a) wet: 1–8 September 1998 and (b) dry: 1–8 December 1998. Triangles represent road sinks (points where on-road flow converges). Circles show the locations of culverts. Broad areas of uniform medium gray are cells with no change.

3.4.4. Stream discharge

Fig. 13 shows hourly road versus non-road stream discharge for the whole 3-year study period. The figure clearly shows that roads increase streamflow in the basin for all storm sizes. Based on the means of each simulation, however, the increase is only 2.7%.

Some individual storm events were examined to better understand road effects on storm flow. Rainfall and streamflow during mid-August–mid-September 1998 are presented in Fig. 14. At 15:00 LT on 15 August when rainfall intensity reached 40 mm h^{-1}, simulated peak flow with roads was

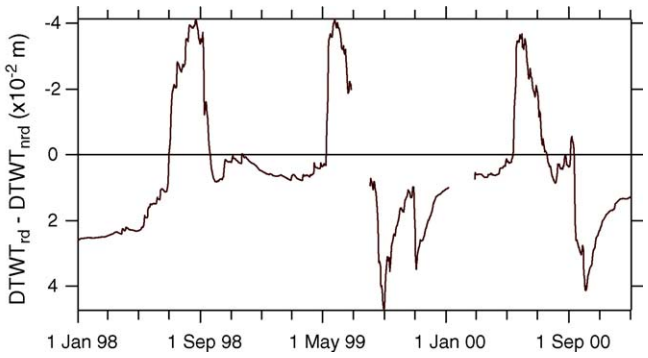

Fig. 12. Time series of basin-averaged road-related depth-to-water-table anomaly (road minus non-road).

514 m^3 h^{-1} higher (+59%) than without roads. When rainfall intensity reached 27 mm h^{-1} at 18:00 LT on 8 September, peak flow was 294 m^3 h^{-1} higher (+33%) with the road.

To further examine the effects of roads on storm hydrographs, road and non-road peak values are compared in Fig. 15. The effects of roads on peak flows can be seen to increase with storm size. Roads increase peak flows by 3, 12, and 34%, respectively, for peak flows of less than 200, 200–800, and greater than 800 m^3 h^{-1}. This result contrasts with the previous finding that road-related Horton overland flow in PKEW has more influence on the stream hydrograph for frequently-occurring small events than for larger events (Ziegler and Giambelluca, 1997), and with many PNW paired watershed studies (Wright et al., 1990; Jones and Grant, 1996; Thomas and Megahan, 1998; Beschta et al., 2000), which found decreasing effects on peak flow as storm size increased. However, some watershed studies (Jones, 2000) and prior road studies using DHSVM (Bowling et al., 2000; Storck et al., 1998) have also found increasing effects of roads with increasing event size.

Our results also show that road effects on peak flow are greater than the effects on total storm volume. For example, for the large storm of 5–9 September 1998, roads increased peak flow by 33%, while total storm volume increased by only 20%. This suggests that the roads in PKEW influence stream behavior not only by increasing overland flow but also by shortening overland flow paths, resulting in much higher peaks.

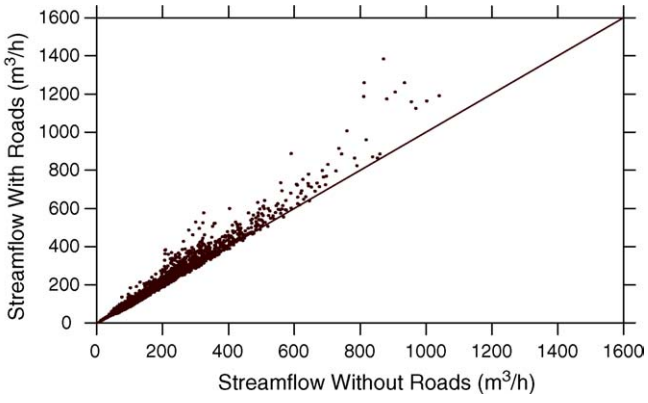

Fig. 13. Scattergram of hourly streamflow for road vs. non-road simulations.

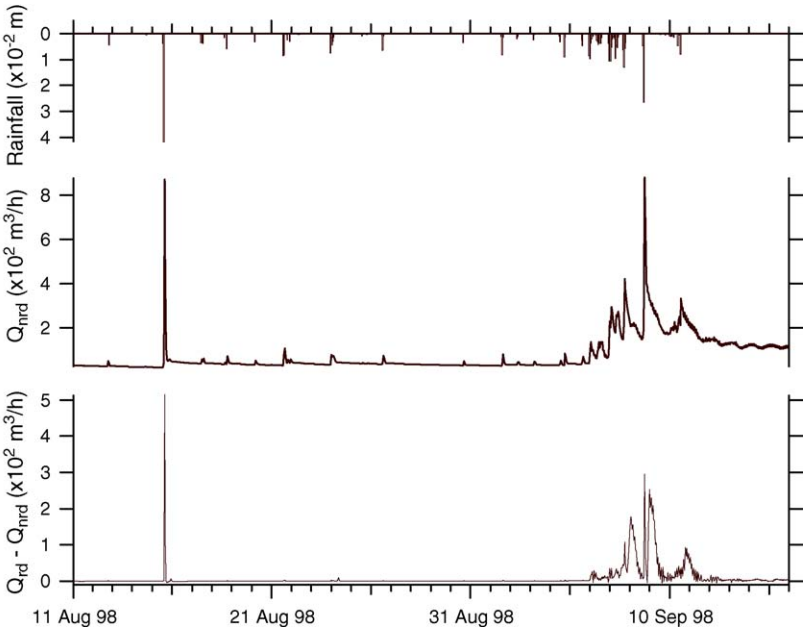

Fig. 14. Rainfall (top), streamflow simulation without road (Q_{nrd}) (middle), and the difference in streamflow between roads and non-roads (Q_{rd} minus Q_{nrd}) (bottom) for sample period 11 August–15 September 1998.

As a result, roads are major contributors to concentrated, erosion-producing overland flow during large events, despite the relatively small area they occupy.

3.4.5. Sustained effects of roads

Over the 3-year simulation period, streamflow is increased on average by about 3% by roads. As required by mass balance, the streamflow increase is compensated by decreases in both ET and water storage change. About half of the streamflow increase during the simulation period was produced at the expense of water storage. However, over the long-term, basin water storage change can be assumed to be negligible with or without the road. Hence, the long-term average difference in water storage change between road and non-road cases is close to zero. For the long-term, then, average streamflow increase due to roads must be equivalent to average ET decrease. The greater streamflow increase seen here is representative only of the relatively short 3-year simulation period. Although a longer simulation would show only a small increase in average streamflow due to the road, there would probably still be significant increases during wet season months because of higher storm flows. Mass balance would therefore require that dry season flows be reduced.

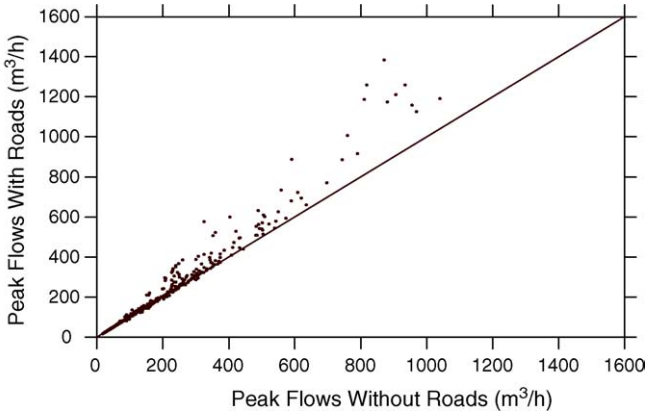

Fig. 15. Scattergram of peak flows for road vs. non-road simulations.

4. Summary and conclusions

We had mixed success in applying DHSVM in the tropical setting of PKEW. Soil moisture at the four measurement sites was well simulated in all three root-zone soil layers. The stream discharge estimate captured the major features of the measured hydrograph. However, the modeled streamflow was reasonably close to observed flow in only 2 of the 3 years of simulation. We believe the discrepancies between observed and simulated flow, particularly for 1999, are the result of changes in land cover or flow diversion not represented in the model.

Based on the model results, the effects of roads in PKEW on the average water balance of the basin are relatively small. ET is reduced, but the average reduction is less than 1%, not surprising given the small proportion of basin area (1.2%) directly affected by roads. The road redistributes soil moisture in nearby and down-slope cells, and also affects depth to water table, with the water table shifted downward under the road and upward where water exits the road.

Despite relatively small effects on the average partitioning of water in the basin, our results suggest that roads may have harmful impacts on water supply and water quality. Increased peak flows due to roads generally have only negative effects. The increased flow during storms is generated on the roads, and results in severe gullying of the road surface (Ziegler et al., 2004). Eroded material is efficiently transported to stream

channels by the roads, contributing significantly to sediment loads. From some sections of the road, concentrated overland flow is directed to hillslopes, damaging crops and eroding soil from farm fields. Also, although this effect is not realized in the relatively short 3-year simulation period, increased storm flows may ultimately be compensated by significant decreases in dry season flow.

As population increases in the region and a market-oriented economy replaces subsistence, vehicle numbers grow, and the rural road network continues to expand and increase in density. This study was done in a small watershed with a relatively low road density. It is reasonable to expect that the effects of roads on peak stream discharge are greater in basins with more relative road area, and will increase through time as the road network expands in basins such as PKEW.

Acknowledgements

This paper is based upon the work supported by the National Science Foundation under grant no. EAR-0000546. Any opinions, findings, and conclusions expressed in this paper are those of the authors and do not necessarily reflect the views of the National Science Foundation. DHSVM authors Dennis Lettenmaier (Department of Civil and Environmental Engineering, University of Washington), Pascal Storck (3TIER Environmental Forecast Group, Seattle, WA, USA), and Laura Bowling (Department of Agronomy, Purdue University) and Bart Nijssen (Hydrology and Water Resources, and Civil Engineering and Engineering Mechanics, University of Arizona) generously supported our efforts to implement DHSVM, by answering our numerous inquiries. Toby Vana (Department of Geography, University of Hawai'i) conducted the vegetation survey and generated the vegetation map used in the simulation.

References

Beckers, J., Alila, Y., 2004. A model of rapid preferential hillslope runoff contributions to peak flow generation in a temperate rain forest watershed. Water Resour. Res. 40, W03501, doi:10.1029/2003WR002582.

Beschta, R.L., Pyles, M.R., Skaugset, A.E., Surfleet, C.G., 2000. Peakflow response to forest practices in the western cascades of Oregon, USA. J. Hydrol. 233, 102–120.

Bowling, L.C., Storck, P., Lettenmaier, D., 2000. Hydrologic effects of logging in western Washington, United States. Water Resour. Res. 36 (11), 3223–3240.

Clapp, R.B., Hornberger, G.M., 1978. Empirical equations for some soil hydraulic properties. Water Resour. Res. 14 (4), 601–604.

Cuo, L., 2005. Effects of land cover and rural roads on hydrological processes in montane watersheds in northern Thailand. Ph.D. Dissertation. Department of Geography, University of Hawai'i at Manoa.

Fox, J., Krummel, J., Yarnasarn, S., Ekasingh, M., Podger, N., 1995. Land use and landscape dynamics in northern Thailand: assessing change in three upland watersheds. Ambio 24 (6), 328–334.

Geist, H.J., Lambin, E.F., 2001. What drives tropical deforestation?—a meta-analysis of proximate and underlying causes of deforestation based on subnational case study evidence, LUCC report series no. 4, Louvain-la-Neuve, Belgium.

Giambelluca, T.W., 1996. Tropical land cover change: charactering the post forest land surface. In: Giambelluca, T.W., Henderson-Sellers, A. (Eds.), Climate Change: Developing Southern Hemisphere Perspectives. John Wiley and Sons, UK, pp. 293–318.

Harr, R.D., Harper, W.C., Krygier, J.T., 1975. Changes in storm hydrographs after road building and clear-cutting in the Oregon Coast Range. Water Resour. Res. 11 (3), 436–444.

Jones, J.A., 2000. Hydrologic processes and peak discharge response to forest removal, regrowth, and roads in 10 small experimental basins, western Cascades, Oregon. Water Resour. Res. 36 (9), 2621–2642.

Jones, J.A., Grant, G.E., 1996. Peak flow responses to clear-cutting and roads in small and large basins, western Cascades, Oregon. Water Resour. Res. 32 (4), 959–974.

Keppeler, E.T., Ziemer, R.R., 1990. Logging effects on streamflow: water yield and summer low flows at Caspar Creek in Northern California. Water Resour. Res. 26 (7), 1669–1679.

King, J.G., Tennyson, L.C., 1984. Alteration of streamflow characteristics following road construction in north central Idaho. Water Resour. Res. 20 (8), 1159–1163.

La Marche, J.L., Lettenmaier, D.P., 2001. Effects of forest roads on flood flows in the Deschutes River, Washington. Earth Surf. Process. Landforms 26, 115–134.

Larkin, E.D., 2002. Radiation balance of over forested and agricultural sites in northern Thailand. Master's Thesis. Geography, University of Hawai'i at Manoa.

Leung, L.R., Wigmosta, M.S., Ghan, S.J., Epstein, D.J., Vail, L.W., 1996. Application of a subgrid orographic precipitation/surface hydrology scheme to a mountain watershed. J. Geophys. Res. 101 (D8), 12803–12817.

Nash, J.E., Sutcliffe, J.V., 1970. River flow forecasting through conceptual models 1, a discussion of principles. J. Hydrol. 10, 282–290.

Nijssen, B., Lettenmaier, D.P., 1999. A simplified approach for predicting shortwave radiation transfer through boreal forest canopies. J. Geophys. Res. 104 (D22), 27859–27868.

Noguchi, S., Tsuboyama, Y., Sidle, R.C., Hosoda, I., 2001. Subsurface runoff characteristics from a forest hillslope soil profile including macropores, Hitachi Ohta. Jpn. Hydrol. Process. 15, 2131–2149.

Rothacher, J., 1970. Increases in water yield following clear-cut logging in the Pacific Northwest. Water Resour. Res. 6 (2), 653–658.

Sidle, R.C., Sasaki, S., Otsuki, M., Noguchi, S., Rahim Nik, A., 2004. Sediment pathways in a tropical forest: effects of logging roads and skid trails. Hydrol. Process. 18, 703–720.

Storck, P., Bowling, L., Wetherbee, P., Lettenmaier, D., 1998. Application of a GIS-based distributed hydrology model for prediction of forest harvest effects on peak stream flow in the Pacific Northwest. Hydrol. Process. 12, 889–904.

Thomas, R.B., Megahan, W.F., 1998. Peak flow responses to clear-cutting and roads in small and large basins, western Cascades, Oregon: a second opinion. Water Resour. Res. 34 (12), 3393–3403.

Thyer, M., Beckers, J., Spittlehouse, D., Alila, Y., Winkler, R., 2004. Diagnosing a distributed hydrologic model for two high-elevation forested catchments based on detailed stand- and basin-scale data. Water Resour. Res. 40, W01103, doi:10.1029/2003WR002414.

Wigmosta, M.S., Burges, S.J., 1997. An adaptive modeling and monitoring approach to describe the hydrologic behavior of small catchments. J. Hydrol. 202, 48–77.

Wigmosta, M.S., Vail, L.W., Lettenmaier, D.P., 1994. A distributed hydrology-vegetation model for complex terrain. Water Resour. Res. 30 (6), 1665–1679.

Wigmosta, M.S., Nijssen, B., Storck, P., 2002. The distributed hydrology soil vegetation model. In: Singh, V.P., Frevert, D.K. (Eds.), Mathematical Models of Small Watershed Hydrology and Applications. Water Resource Publications, Littleton, CO, pp. 7–42.

Wigneron, J.-P., Olioso, A., Calvet, J.-C., Bertuzzi, P., 1999. Estimating root zone soil moisture from surface soil moisture data and soil-vegetation-atmosphere transfer modeling. Water Resour. Res. 35 (12), 3735–3745.

Wright, K.A., Sendek, K.H., Rice, R.M., Thomas, R.B., 1990. Logging effects on streamflow: storm runoff at Caspar Creek in Northwestern California. Water Resour. Res. 26 (7), 1657–1667.

Ziegler, A.D., 2000. Toward modeling erosion on unpaved roads in mountainous Northern Thailand. Ph.D. Dissertation. University of Hawaii at Manoa, Hawaii, US.

Ziegler, A.D., Giambelluca, T.W., 1997. Importance of rural roads as source areas for runoff in mountainous areas of northern Thailand. J. Hydrol. 196, 204–229.

Ziegler, A.D., Sutherland, R.A., Giambelluca, T.W., 2000. Runoff generation and sediment production on unpaved roads, footpaths, and agricultural land surfaces in northern Thailand. Earth Surf. Process. Landforms 25, 519–534.

Ziegler, A.D., Giambelluca, T.W., Sutherland, R.A., Vana, T.T., Nullet, M.A., 2001a. Horton overland flow contribution to runoff on unpaved mountain roads: a case study in northern Thailand. Hydrol. Process. 15, 3203–3208.

Ziegler, A.D., Sutherland, R.A., Giambelluca, T.W., 2001b. Interstorm surface preparation and sediment detachment by vehicle traffic on unpaved mountain roads. Earth Surf. Process. Landforms 26, 235–250.

Ziegler, A.D., Giambelluca, T.W., Sutherland, R.A., Nullet, M.A., Yarnasarn, S., Pinthong, J., Jaiaree, S., 2004. Toward understanding the cumulative impacts of roads in agricultural watersheds of northern Thailand. Agric. Ecosyst. Environ. 104, 145–158.

Ziemer, R.R., 1981. Storm flow response to road building and partial cutting in small streams of northern California. Water Resour. Res. 17 (4), 907–917.